Operation of Parallel Grid-Supporting PVs

Sulaiman Almutairi
Electrical Engineering Department
University of South Florida
Tampa FL 33620 USA
Email: sza@mail.usf.edu

Zhixin Miao
Electrical Engineering Department
University of South Florida
Tampa FL 33620 USA
Email: zmiao@usf.edu

Lingling Fan
Electrical Engineering Department
University of South Florida
Tampa FL 33620 USA
Email: linglingfan@usf.edu

***Abstract*—In this paper, we investigate operation of multiple solar photovoltaic (PVs) in utility grid integration and islanded microgrid. Two PVs are considered and the grid-supporting inverters are adopted for the two PVs. The PVs are able to work in both utility grid and microgrid with the same control scheme. The control scheme is based on the conventional P-f and Q-v droop control strategy. Smooth transition between grid-connected to islanded mode is achieved. Moreover, we investigate the effect of load transients during stand-alone operation on PV performance, including dc side voltages. The investigation is carried out by computer simulation of two parallel-connected PV inverters in Matlab/SimPowerSystems environment. Two operation cases, grid-connected and transition to islanded mode, are presented.**

***Index Terms*—microgrid, photovoltaic (PV), grid-supporting, stand alone operation, Grid-connected mode, droop control,Voltage-source control**

I. Introduction

Today's power system has more and more renewable energy penetration [1] [2]. The integration of renewable energy sources to the grid brings many benefits, such as reduction of peak demand and enhancement of power quality and reliability. With the high penetration of distributed generator sources (DG), the concept of microgrid is introduced [3]. A microgrid can be characterized as an interconnection of loads and DG sources such as PV sources, wind-turbines and energy storage systems (ESS). The microgirds can operate in two operation modes, grid-connected or islanded mode [4]. An appropriate control of microgrids is required to ensure stable and coordinated operations among grid source, DGs and distributed loads.

DGs interface to the microgrid through DC/AC inverters. Different types of inverter control have been investigated in the literature, e.g., [5]–[7]. They can be categorized into three basic types, grid-feeding, grid-forming and grid-supporting. The grid feeding inverter operates as a current source. It is suitable to work in grid-connected mode. This inverter regulates the active and reactive power based on pre-defined setting values. On the other hand, the grid-forming inverter is more practical to operate autonomously. It works as a voltage source. The objectives of this inverter are to maintain the voltage at the point of common coupling (PCC) bus and system frequency at referenced point [7]. Finally, the grid-supporting inverter has the objectives of both grid-feeding and grid-forming inverters. The control of the inverter is based on the conventional P-f and Q-V droop control strategy [7], [8]. It can be functioned as a current or voltage source. In case of a current source, a switching to grid-forming mode is needed to operate in islanded-mode. However, if it is implemented as a voltage source, it can work in both connected to or islanded from the grid which eliminates the need for switching.

Driven by several factors, such as low maintenance and high reliability, photovoltaic systems (PV) are attracting more interests in microgrid applications. Most of the conventional PV inverters control adopt grid-following control to send out maximum power to grid or microgrid. Voltage and frequency control is usually enforced by a battery in a microgrid. On the other hand, applying grid-forming control to PV inverters may save the cost of purchasing a battery. Thus, grid-forming control of PV inverters has been researched recently.

In 2008, a single-phase 240 V ac 5 kVA PV inverter was designed in laboratory to work as a voltage source or grid-forming mode [9]. In the CERTs microgrid project, three-phase grid-forming PV inverter was adopted, indicated in a paper in 2011 [10]. Due to PV's limited power generation capability, it is found that when grid-forming PV makes up power requirement greater than PV's maximum power capacity, PV's dc voltage suffers collapse [11]. A minimum dc voltage control for PV grid-forming inverters is also designed in [11] to lower its frequency in a much quicker fashion so that other energy sources can pick up power quickly. This strategy can then relieve grid-forming inverter overloading. The strategy is also demonstrated in CERTS/AEP microgrid test bed [12].

In this paper, we investigate the performance of the voltage source grid-supporting inverter with two parallel-connected PV sources in a microgrid. The control is designed and tested with two cases, grid-connected and transition to islanded modes. It will be shown that the control is able to achieve reliable results. Smooth transition between the two operation modes is achieved because there is no need of changing the inverter control algorithm. Moreover, during islanded mode operation, the microgrid may encounter load transient. This load transient may lead to overloading of the inverter and cause the DC-link voltage to collapse. The impact of such a scenario in the DC-link voltage during stand-alone operation is also investigated.

978-1-7281-0407-2/19/$31.00 ©2019 IEEE

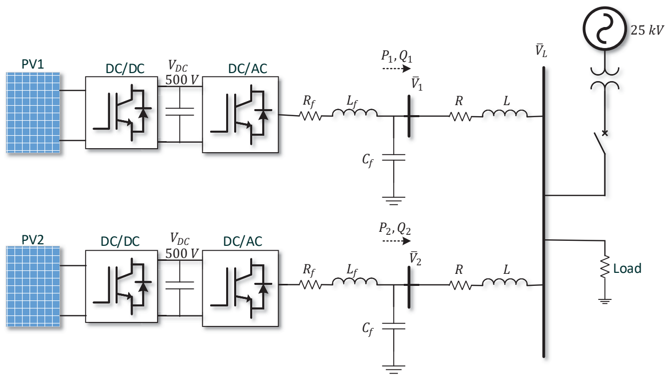

Fig. 1: Microgrid Configuration.

The remainder of the paper is organized as follows. Microgrid structure and the overall control configuration of the voltage source grid-supporting inverter is demonstrated in Section II. Case study simulation results are presented and analyzed in Section III. Conclusions are provided in Section IV.

II. SYSTEM STRUCTURE AND CONTROL

This section describes the PV-based microgrid structure and its inverter control. First, the structure of the microgrid is described; then, the control is illustrated.

A. Microgrid Structure.

Fig. 1 shows the microgrid diagram, including two PV units and loads connected to the main grid through a switch. The microgrid can operate in both, grid-connected or islanded mode.

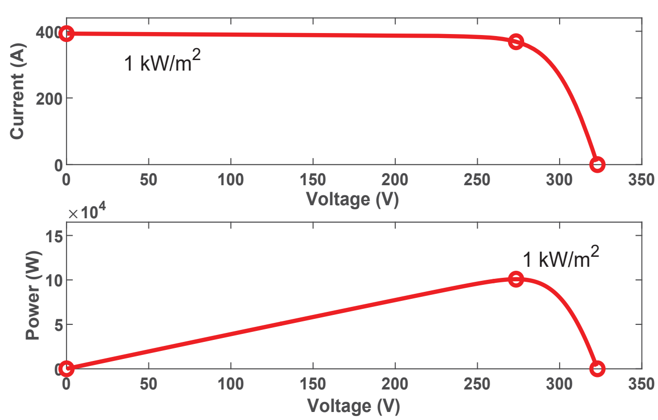

Fig. 2: PV panels characteristic curves.

In this paper, PV systems with two-stage power conversion configuration including a DC-DC boost converter to boost dc voltage, and a DC-AC inverter to convert dc to ac, is chosen. Each single PV unit delivers a maximum power generation of 100 kW. The PV panels characteristic curves, current verses Voltage (I-V) and power verses voltage (P-V) are shown in Fig. 2 [13].

The DC-DC boost converter is used to boost the PV voltage V_{ph} to a specified voltage along with harvesting the maximum power from PV panels. Maximum Power Point Tracking (MPPT) algorithm is widely used in commercial PV systems [14]–[17]. The MPPT method generates the desired voltage in order to obtain the maximum power by varying the DC converter duty cycle. Perturb and Observer, the commonly adopted MPPT algorithm, is implemented in the testbed.

B. Control of VSI

A detailed control structure of the voltage source grid-supporting inverter is presented in Fig. 3 [18]. The overall control contains several control blocks, real and reactive power calculation, droop control, voltage control, and current control. Complete configuration of the control blocks are demonstrated in Fig. 4 and Fig. 5. Explanation of the controls is given below.

1) Power Calculation

The real and reactive power can be calculated based on equation and [6], [7].

$$P = \frac{3}{2}(V_d i_d + V_q i_q) \tag{1}$$

$$Q = \frac{3}{2}(V_q i_d - V_d i_q) \tag{2}$$

where, V_d and V_q are the three phase terminal (capacitor) voltage V_{abc} in dq frame, i_d and i_q are the inverter output current i_{abc} in dq frame, where they are calculated based on the Park Transformation.

2) Droop Control

The inverter droop control is based on the the conventional P-f and Q-V droop controller and shown in Fig. 4.

$$\omega^* = \omega_n + M_p(P^* - P) \tag{3}$$

$$E^* = V_n + M_q(Q^* - Q) \tag{4}$$

where P^* and P are the referenced and actual real power, Q^* and Q are the referenced and actual reactive power, E^* and V_n are referenced and nominal voltage, ω and ω_n are the referenced and nominal frequency, and M_p and M_q are the droop coefficient. The control of the droop is depicted in Fig. 4.

Droop control makes sure that the inverter's frequency and voltage will increase if real and reactive power decrease.

3) Voltage and Current Control

Fig. 5 shows the voltage and current control. The voltage reference signal is acquired by subtracting the voltage drop on the virtual impedance from the original referenced value obtained from the droop control:

$$V_{ref} = E^* - i_d Z_v \tag{5}$$

Z_v the virtual impedance which is implemented to enhance the power sharing. The real and reactive power are controlled by regulating the inverter output current i_d and i_q.

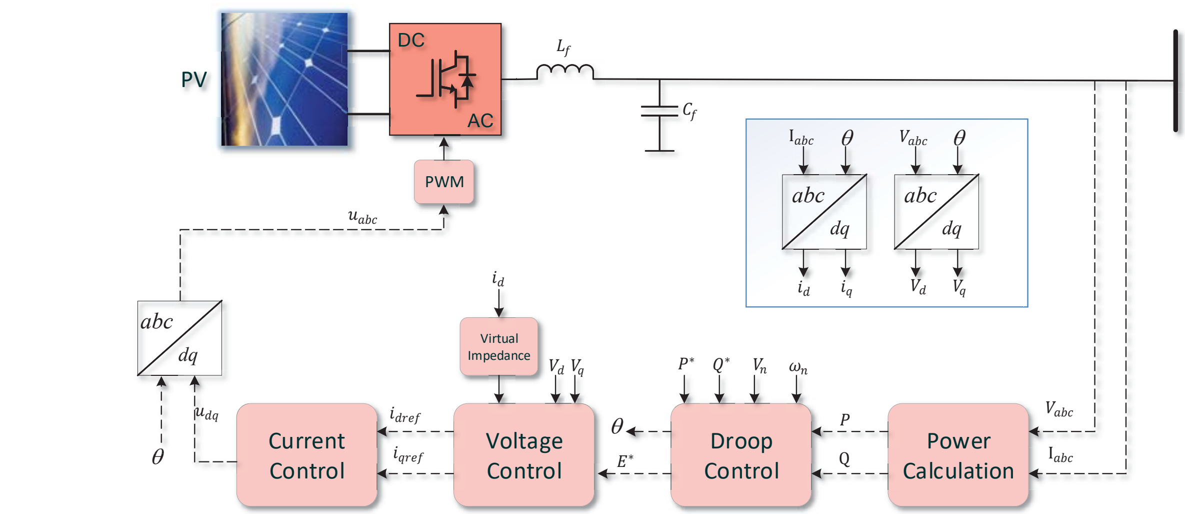

Fig. 3: Control structure of the voltage source grid-supporting inverter.

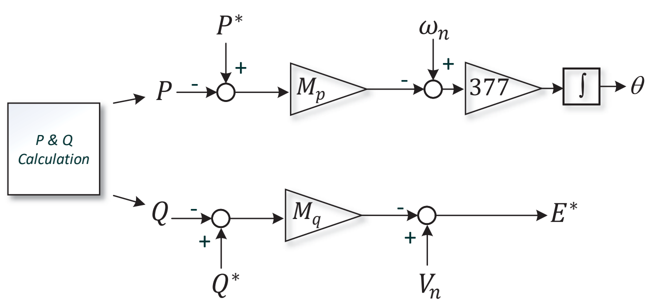

Fig. 4: Droop Control.

The referenced signals of the inverter output current, i_{dref} and i_{qref}, are produced from the voltage control loop after a proportional-integral (PI) control which are derived in (6).

$$\begin{aligned} i_{dref} &= \left[K_{p1} + \frac{K_{i1}}{s}\right](E^* - V_v - V_d) \\ i_{qref} &= \left[K_{p1} + \frac{K_{i1}}{s}\right](-(I_d R_v + V_q)) \end{aligned} \tag{6}$$

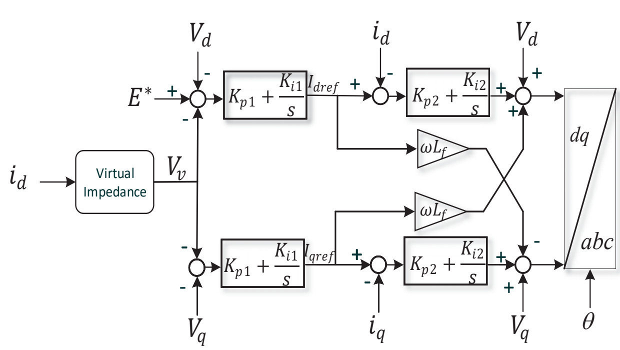

Fig. 5: Voltage and current Control.

The current control loop, which is shown in Fig. 5, generates the voltage signals u_d and u_q in $d-q$ frame. These compensated voltages are transformed into abc frame and fed to Pulse-width-modulation (PWM) to generate control signals for the voltage-source inverter. u_d and u_q are expressed as in equations (7) and (8).

$$u_d = \left[K_{p2} + \frac{K_{i2}}{s}\right](i_{dref} - i_d) - \omega L_f i_q + V_d \tag{7}$$

$$u_d = \left[K_{p2} + \frac{K_{i2}}{s}\right](i_{qref} - i_q) - \omega L_f i_d + V_q \tag{8}$$

III. Results

The microgrid shown in Fig. 1 is implemented in Matlab/SimPowerSystems environment in order to analyze the performance of the described control. Two operation modes, grid-connected mode and transition to islanded-mode, are considered in the study. The system parameters are presented on Table I.

A. Grid-connected mode

During grid-connected mode, both PV units operate at their maximum power generation rating with MPPT method. They supply the local loads and the excessive power is exported into the grid. The simulation results are shown in Fig. 6.

Fig. 6(a) presents the active and power from both PV sources, the grid, and the load. As it can be observed from the results, at the first stage, both PVs supply maximum power generation at 100 kW. Since the load demand is less than the PVs power generation, the excessive power, which is 50 kW, is fed to the grid. At $t = 4$ s , the load is increased from 150 kW to 250 kW, the load demand becomes more than the PV capabilities. Therefore, the grid picks up the load and imports power to the microgrid to supply the load.

TABLE I: System Parameters

Discription	Parameters	Value
Power base	S_b	200 kW
Voltage base	ac side	260V, 25 kV
Voltage base	dc side	500 V
System frequency	f	60 Hz
	R_f	0.0055 pu
Inverter filter	L_f	0.0981 pu
	C_f	0.25 pu
feeder parameters	R	0.0046 pu
	L	0.0045 pu
	K_{p1}/K_{i1}	1/100
Control parameters	K_{p2}/K_{i2}	0.3/20
	Z_v	0.01 pu
Droop parameters	M_p	0.0053 pu
	M_q	0.05 pu

Fig. 6(b) shows the dynamic of the DC-link voltage with small change when the load rises. The voltage and the system frequency at the PCC bus are shown in Fig. 6(c) and (d). As shown in the figure, both voltage and frequency are kept constant, except small variation during the variation during the change in load demand.

Therefore, based on the shown results above, it can be concluded that the power balance and the operation of the control in the microgrid is achieved during grid-connected mode.

B. Transition to islanded-mode

In this case, we examined the interaction between the parallel PV sources after an intentional transition to islanded-mode. In the stand-alone mode, frequency and voltage are dependent on the PV sources only. Fig. 7 presents the simulation results.

Before the transition, both PV sources outputs 200 kW, the load is 150 kW and 50 kW is imported to the grid. The transition occurs at $4\ s$. In Fig. 7(a), dynamic responses of the two PV inverters, the grid source, the DC-link voltage, the PCC voltage and the frequency before and after the transition are demonstrated. After the transition, the grid power becomes zero. Each PV source backs off its output power by 25 kW or 0.125 pu for a 200 kW power base. Since the droop parameter M_p is 0.0053 pu, we expect to see frequency rise of $0.125 \times 0.0053 \times 60 = 0.04$ Hz.

Fig. 7(a) presents the real power dynamic responses. Once the microgrid is islanded from the main grid, the two PV sources automatically decrease their output power generation based on the load demand. The load is evenly shared between the two sources.

Fig. 7(b) demonstrates the DC-link voltage response. After the microgrid is disconnected, it is observed that the DC-link

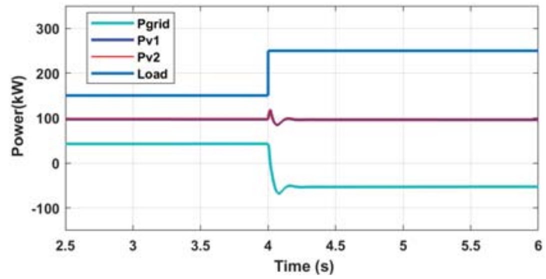

(a)

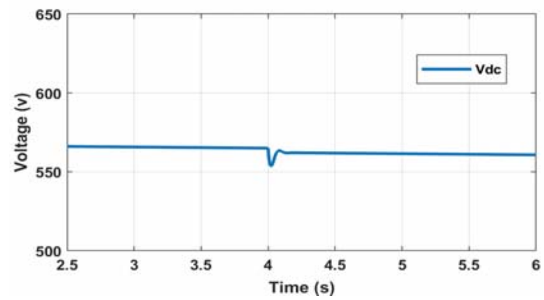

(b)

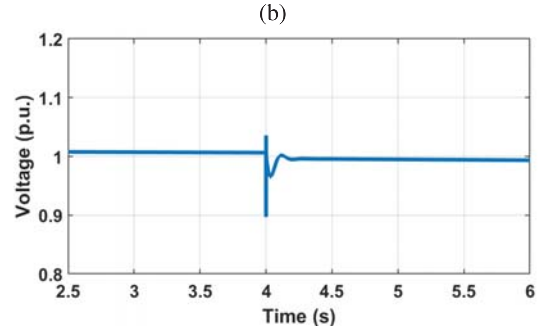

(c)

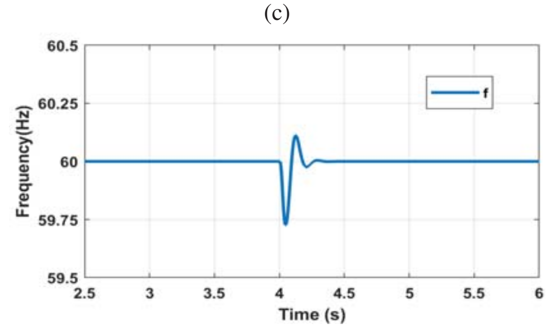

(d)

Fig. 6: Dynamic responses during grid-connected mode. (a) Active power, (b) DC-link Voltage, (c) PCC bus voltage magnitude, (d) System frequency.

voltage increases in response to decreased power generated for each PV inverter.

Fig. 7(c) and (d) depicts the voltage and frequency responses at the PCC bus respectively. During the transition, the results show smooth transition on both voltage and frequency. As it can be seen, the frequency increases to 60.04 Hz and stay at steady state. The observation corroborates with the analysis that predicts 0.04 Hz increase in frequency.

The case study results demonstrate that the grid-supporting

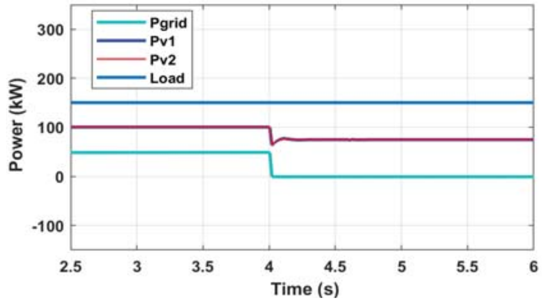

(a)

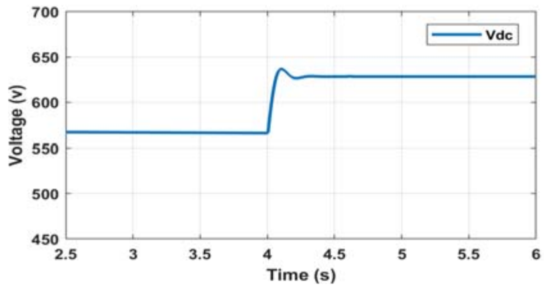

(b)

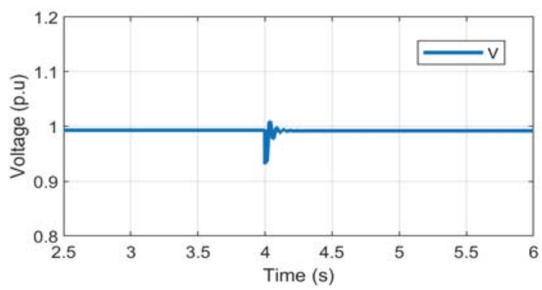

(c)

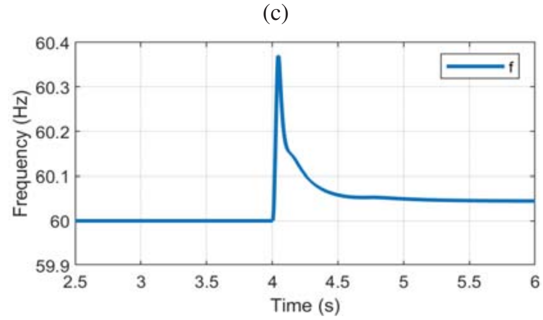

(d)

Fig. 7: Dynamic responses during transition to islanded-mode. (a) Active power, (b) DC-link Voltage, (c) PCC bus voltage magnitude, (d) System frequency.

converters can operate as expected during transition.

C. DC-link during transient load

During islanded mode operation, the microgrid may encounter sudden load increase which can exceed the PV generation capabilities. This issue may cause disturbances to the DC-link voltage. It could lead to voltage collapse and trip of the inverter. The PI-controller limiters have influence during the load transient which can prevent the inverter from collapsing. Two cases are considered to analyze the effect of overloading on the DC-link voltage. The first case considers the impact with the presence of the PI-controller limiters in voltage contrl that generates the current reference and the second one considers the same impact without these limiters. The simulation results are depicted in Figs. 8 and 9.

Fig. 8 shows the first case. Before $t = 2$ s, the two PV inverters were supplying a 150 kW load demand which is within their generation limits. At $t = 2$ s, a sudden 100 kW load changed is applied. As it can be seen from Fig. 8(a), the voltage drops until 290 v then becomes stable after the controller reaches its limit. The PI-controller limiters prevent the voltage from collapsing. Fig. 9 demonstrates the second case with the same scenario. It is noted that at $t = 2$ s, the voltage drops until it collapses which shows the importance of the controller limiters.

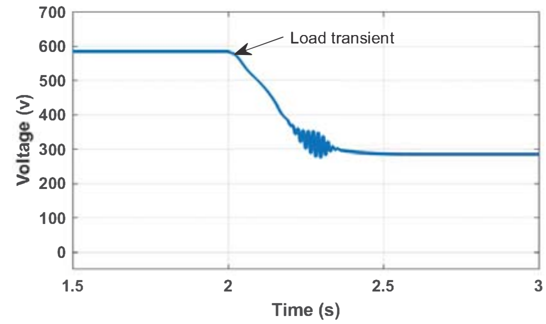

(a)

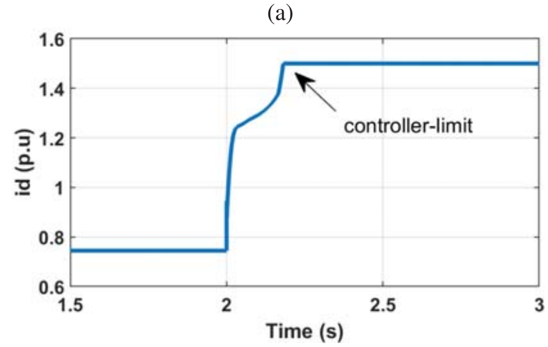

(b)

Fig. 8: Dynamic responses during load transient with controller-limits: a) DC-link voltage, b) i_d.

IV. Conclusion

In this paper, the voltage source grid-supporting PV inverters for two parallel-connected PV sources in a microgrid is presented. The grid-supporting control has the capability to operate in both grid-connected and islanded modes. A Matlab/SimPowerSystems testbed is built to analyze the feasibility of the control. The presented simulation results demonstrate that the reliability of the described control. Smooth transition between the two operation modes is achieved using the grid-supporting inverters. Furthermore, load transient effect on the DC-link voltage is investigated.

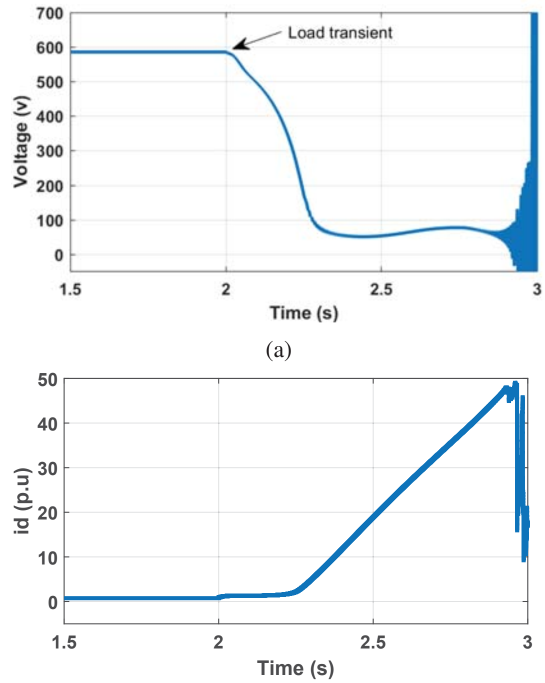

(a)

(b)

Fig. 9: Dynamic responses during load transient without controller-limits: a) DC-link voltage, b) i_d.

The load transient could influence the stability of the inverter. The results indicate that the embedded PI-controller limits prevents the voltage from collapsing when the inverter is overloaded.

References

[1] B. Kroposki, B. Johnson, Y. Zhang, V. Gevorgian, P. Denholm, B.-M. Hodge, and B. Hannegan, "Achieving a 100% renewable grid: Operating electric power systems with extremely high levels of variable renewable energy," *IEEE Power and Energy Magazine*, vol. 15, no. 2, pp. 61–73, 2017.

[2] M. Datta, T. Senjyu, A. Yona, T. Funabashi, and C.-H. Kim, "A frequency-control approach by photovoltaic generator in a pv–diesel hybrid power system," *IEEE Transactions on Energy Conversion*, vol. 26, no. 2, pp. 559–571, 2011.

[3] J. He and Y. W. Li, "An enhanced microgrid load demand sharing strategy," *IEEE Transactions on Power Electronics*, vol. 27, no. 9, pp. 3984–3995, 2012.

[4] A. Bidram and A. Davoudi, "Hierarchical structure of microgrids control system," *IEEE Transactions on Smart Grid*, vol. 3, no. 4, pp. 1963–1976, 2012.

[5] J. Rocabert, A. Luna, F. Blaabjerg, and P. Rodríguez, "Control of power converters in AC microgrids," *IEEE Transactions on Power Electronics*, vol. 27, no. 11, pp. 4734–4749, 2012.

[6] A. Yazdani and R. Iravani, *Voltage-sourced converters in power systems*. Wiley Online Library, 2010, vol. 34.

[7] L. Fan, *Control and dynamics in power systems and microgrids*. CRC Press, 2017.

[8] X. Yu, A. M. Khambadkone, H. Wang, and S. T. S. Terence, "Control of parallel-connected power converters for low-voltage microgridpart i: A hybrid control architecture," *IEEE Transactions on Power Electronics*, vol. 25, no. 12, pp. 2962–2970, 2010.

[9] J. C. Vasquez, R. A. Mastromauro, J. M. Guerrero, and M. Liserre, "Voltage support provided by a droop-controlled multifunctional inverter," *IEEE Transactions on Industrial Electronics*, vol. 56, no. 11, pp. 4510–4519, 2009.

[10] M. J. Erickson, T. Jahns, and R. H. Lasseter, "Comparison of pv inverter controller configurations for certs microgrid applications," in *2011 IEEE Energy Conversion Congress and Exposition*. IEEE, 2011, pp. 659–666.

[11] W. Du, Q. Jiang, M. J. Erickson, and R. H. Lasseter, "Voltage-source control of pv inverter in a certs microgrid," *IEEE Transactions on Power Delivery*, vol. 29, no. 4, pp. 1726–1734, 2014.

[12] W. Du, R. H. Lasseter, and A. S. Khalsa, "Survivability of autonomous microgrid during overload events," *IEEE Transactions on Smart Grid*, pp. 1–1, 2018.

[13] [Online]. Available: https://www.mathworks.com/help/physmod/sps/examples/average-model-of-a-100-kw-grid-connected-pv-array

[14] S. Kouro, B. Wu, H. Abu-Rub, and F. Blaabjerg, "Photovoltaic energy conversion systems," *Power Electronics for Renewable Energy Systems, Transportation and Industrial Applications*, pp. 160–198, 2014.

[15] Y. Yang, K. A. Kim, F. Blaabjerg, and A. Sangwongwanich, *Advances in Grid-Connected Photovoltaic Power Conversion Systems*. Woodhead Publishing, 2018.

[16] A. Tazay and Z. Miao, "Control of a three-phase hybrid converter for a pv charging station," *IEEE Transactions on Energy Conversion*, vol. 33, no. 3, pp. 1002–1014, 2018.

[17] J. Khazaei, Z. Miao, L. Piyasinghe, and L. Fan, "Real-time digital simulation-based modeling of a single-phase single-stage pv system," *Electric Power Systems Research*, vol. 123, pp. 85–91, 2015.

[18] A. Vinayagam, K. Swarna, S. Y. Khoo, A. T. Oo, and A. Stojcevski, "Pv based microgrid with grid-support grid-forming inverter control-(simulation and analysis)," *Smart grid and renewable energy*, vol. 8, no. 01, pp. 1–30, 2017.